MOLECULAR BIOLOGY

Wnt signaling activates MFSD2A to suppress vascular endothelial transcytosis and maintain blood-retinal barrier

Zhongxiao Wang[1], Chi-Hsiu Liu[1], Shuo Huang[1], Zhongjie Fu[1], Yohei Tomita[1], William R. Britton[1], Steve S. Cho[1], Chuck T. Chen[2], Ye Sun[1], Jian-xing Ma[3], Xi He[4], Jing Chen[1]*

Breakdown of the blood-retinal barrier (BRB) causes retinal edema and vision loss. We investigated the role of Wnt signaling in maintaining the BRB by limiting transcytosis. Mice lacking either the Wnt co-receptor low-density lipoprotein receptor–related protein 5 ($Lrp5^{-/-}$) or the Wnt ligand Norrin ($Ndp^{y/-}$) exhibit increased retinal vascular leakage and enhanced endothelial transcytosis. Wnt signaling directly controls the transcription of an endothelium-specific transcytosis inhibitor, major facilitator superfamily domain–containing protein 2a (MFSD2A), in a β-catenin–dependent manner. MFSD2A overexpression reverses Wnt deficiency–induced transcytosis in endothelial cells and in retinas. Moreover, Wnt signaling mediates MFSD2A-dependent vascular endothelium transcytosis through a caveolin-1 (CAV-1)–positive caveolae pathway. In addition, levels of omega-3 fatty acids are also decreased in Wnt signaling–deficient retinas, reflecting the basic function of MFSD2A as a lipid transporter. Our findings uncovered the Wnt/β-catenin/MFSD2A/CAV-1 axis as a key pathway governing endothelium transcytosis and inner BRB integrity.

INTRODUCTION

The light-sensing retina is a part of the central nervous system (CNS) and a physiological analog of the brain. Proper visual function requires a stable homeostatic microenvironment in the retina that is efficient for oxygen and nutrient transportation and free of blood-borne toxins. Maintenance of this environment in the inner retina is achieved by the blood-retinal barrier (BRB), which is formed by mature retinal endothelial cells (ECs) as a continuous, nonfenestrated vascular system between the blood and neuronal tissue (*1*). Retinal ECs have two properties essential for their barrier features: (i) specialized tight junction complexes for preventing paracellular flux and (ii) very low rates of vesicular trafficking, known as transcytosis, for limiting transcellular transport (*2*–*4*). Whereas the role of tight junctions in the retinal vascular barrier has been extensively studied (*5*, *6*), the regulation of vascular endothelium transcytosis has only recently been identified as a pivotal factor in maintaining BRB integrity (*4*, *7*, *8*). Breakdown of the BRB is a major cause of retinal edema and resultant vision loss in vascular eye diseases such as diabetic retinopathy (*9*, *10*). In these pathological conditions, increased transcytosis and subsequent increased osmotic pressure are suggested to be main contributors to retinal edema (*10*). However, the exact molecular mechanisms governing EC transcytosis across the BRB remain poorly understood.

In the current study, we explored the mechanisms governing retinal EC transcytosis and BRB integrity using mice lacking the low-density lipoprotein receptor–related protein 5 (*Lrp5*) and its ligand Norrin (encoded by the Norrie disease protein gene, *Ndp*) as experimental models of retinal vascular leakage (*11*–*13*). The *Lrp5* knockout ($Lrp5^{-/-}$) and *Ndp* knockout ($Ndp^{y/-}$) mice, both exhibiting high vascular permeability, are mouse models for two rare genetic eye diseases—familial exudative vitreoretinopathy (FEVR) and Norrie disease, respectively (*11*, *13*–*15*). FEVR patients have delayed and incomplete development of retinal blood vessels, with varying degrees of disease severity, whereas in the more severe X-linked Norrie disease, the retina is massively gliotic and mostly destroyed by the time of birth. Both disease are linked with mutations in an interrelated Wnt signaling pathway involving the ligand Norrin (encoded by the Norrie disease protein gene, *Ndp*), the receptor Frizzled4, and the co-receptor LRP5 (*15*). Both $Lrp5^{-/-}$ and $Ndp^{y/-}$ mice mimic human diseases and exhibit defective and incomplete retinal angiogenesis and the absence of intralaminar (intermediate and deep layers of) retinal vessels, followed by hypoxia-induced pathologic vascular growth in the superficial plexus with glomeruloid vascular structures, persistence of hyaloid vessels, and BRB breakdown (*11*, *13*, *16*–*18*).

The Wnt signaling pathway is important in both embryonic development and pathogenesis of diseases including cancer (*12*, *19*, *20*). Under normal conditions, the ligand Norrin binds with LRP5 and Frizzled4, thereby leading to the stabilization of β-catenin, which translocates to the nucleus to bind nuclear T cell factor/lymphoid enhancer factor (TCF/LEF), and subsequently activating target genes (*21*). However, when the ligands or the receptors are dysfunctional, β-catenin is phosphorylated and targeted for degradation, hence inactivating the canonical Wnt signaling pathway. The Wnt signaling pathway has long been linked to the breakdown of the blood-brain barrier (BBB) and BRB (*22*). Wnt3, Wnt7a/b, and a coactivator of Wnt7a/b, GPR124, promote angiogenesis and barriergenesis through the activation of the Wnt/β-catenin signaling pathway in ECs (*23*–*27*). As such, Wnt signaling is crucial for the formation of the BBB and BRB (*23*, *25*, *28*) in an EC autonomous manner (*28*, *29*). Our previous studies using an $Lrp5^{-/-}$ mouse model of FEVR established that LRP5, through the Wnt signaling pathway, is an essential regulator of BRB integrity and developmental angiogenesis, in part through its regulation of claudin 5, a tight junction

[1]Department of Ophthalmology, Boston Children's Hospital, Harvard Medical School, 300 Longwood Avenue, Boston, MA 02115, USA. [2]Section on Nutritional Neuroscience, National Institute on Alcohol Abuse and Alcoholism, National Institutes of Health, 5625 Fishers Lane, Room 3N-01, North Bethesda, MD 20852, USA. [3]Department of Physiology, The University of Oklahoma Health Sciences Center, Oklahoma City, OK 73104, USA. [4]The F.M. Kirby Neurobiology Center, Boston Children's Hospital, Department of Neurology, Harvard Medical School, Boston, MA 02115, USA.
*Corresponding author. Email: jing.chen@childrens.harvard.edu

protein (*16*, *30*). Other studies also established that low Wnt/β-catenin signaling causes leaky vessels and affects water homeostasis in the BBB (*31*), and that Norrin interplays with Wnt7a/7b in BBB and BRB formation (*32*). However, most of these previous studies on Wnt signaling in vascular barriers have focused on tight junction regulation without examining EC transcytosis, and the mechanisms underlying Wnt-dependent regulation of vascular barrier formation are still not fully understood.

This project studied whether the Wnt signaling pathway may limit EC transcytosis via the major facilitator superfamily domain–containing protein 2a (MFSD2A), a negative regulator of transcytosis, to maintain the BRB. MFSD2A is an endothelium-enriched membrane lipid [docosahexaenoic acid (DHA)] transporter that participates in the regulation of the BBB (*7*, *33*). Loss of MFSD2A in the brain causes increased vascular permeability and BBB breakdown, with increased EC transcytosis in mice and in zebrafish (*34*), whereas lipid transport by MFSD2A helps create a lipid-enriched environment that suppresses caveolar vesicles and EC transcytosis (*35*). Targeted inhibition of MFSD2A has been suggested as a potential route to temporarily disinhibit transcytosis across the BBB (*36*). Here, we showed that the absence of Wnt signaling leads to inner BRB breakdown and high levels of retinal EC transcytosis and caveolar vesicles, as visualized by electron microscopy. Modulation of Wnt signaling in retinal vascular ECs alters transcytosis levels. Moreover, Wnt signaling deficiency in the retinal vascular endothelium results in suppressed levels of MFSD2A. In addition, we identified MFSD2A as a direct TCF- and β-catenin–responsive transcriptional target of Wnt signaling. Last, overexpression of MFSD2A reversed the effects of Wnt signaling on EC transcytosis and caveolar vesicles. A retinal lipid profile analysis also revealed decreased omega-3 fatty acid composition in Wnt-deficient retinas, which is consistent with the lipid transportation role of MFSD2A, as MFSD2A deficiency leads to approximately 50% reduction of retinal DHA (*33*). Together, our findings indicate that the Wnt pathway is an essential regulator of the inner BRB through the regulation of MFSD2A-mediated EC caveolar transcytosis, and that Wnt signaling is also a previously unknown pathway for facilitating lipid transportation in the retina.

RESULTS

BRB integrity is broken down in *Lrp5*- and *Ndp*-deficient eyes

Wnt signaling–deficient mice, *Lrp5* and *Ndp* knockout mice, were analyzed for their BRB integrity using fundus fluorescein angiography (FFA) (Fig. 1A). $Ndp^{y/-}$ mice and male controls ($Ndp^{y/+}$) were used due to the nature that the *Ndp* gene is X-linked, whereas $Lrp5^{-/-}$ mice in the C57BL/6J background were compared with C57BL/6J wild-type (WT) mice. In both $Lrp5^{-/-}$ and $Ndp^{y/-}$ eyes, severe vascular leakage was observed through FFA, thereby suggesting the occurrence of BRB breakdown, whereas in their respective WT controls, fluorescein was confined to retinal vessels and the BRB remained intact (Fig. 1A). In addition, BRB integrity was quantified by measuring the leakage of a large molecule tracer [fluorescein isothiocyanate (FITC)–conjugated 70-kDa dextran] in retinal flat mounts after retro-orbital injection of tracer, costained with a vascular endothelium marker isolectin B_4 (IB_4). The fluorescent tracer was constrained to the IB_4-positive vessels of control retinas; however, substantial leakage was observed from the IB_4-positive vessels of $Lrp5^{-/-}$ and $Ndp^{y/-}$ retinas, which also exhibited pathological glomeruloid vascular structures (Fig. 1B). There was a significant increase in leakage intensity in both knockouts versus their WT control mice (Fig. 1B). These findings of increased vascular permeability in both $Lrp5^{-/-}$ and $Ndp^{y/-}$ retinas suggest the breakdown of BRB integrity in the absence of Wnt signaling.

$Lrp5^{-/-}$ and $Ndp^{y/-}$ retinal vascular endothelia contain high levels of functional transcytotic vesicles

To assess whether Wnt signaling affects EC transcytosis, we next used transmission electron microscopy (TEM) to visualize transcytotic vesicles in $Lrp5^{-/-}$ and $Ndp^{y/-}$ retinal endothelia. For quantification, the trans-endothelial vesicles were categorized into three groups: Type 1 vesicles are those starting to form by endocytosis at the luminal side; type 2 vesicles are those fully formed vesicles being transported inside the cytoplasm; and type 3 vesicles are those being released by exocytosis on the abluminal side. There are substantially increased numbers (by two- to threefold) of all three types of transcytotic vesicles in both $Lrp5^{-/-}$ and $Ndp^{y/-}$ retinas compared with their respective controls (Fig. 1, C and D), suggesting higher levels of retinal EC transcytosis in the absence of Wnt signaling.

To further investigate whether the observed EC vesicles originated from the EC lumen side and may transport circulating substances functionally, horseradish peroxidase (HRP) was retro-orbitally injected into $Lrp5^{-/-}$ and $Ndp^{y/-}$ mice and their littermate controls (WT and $Ndp^{y/+}$). Retinal sections were stained with an HRP colorimetric 3,3′-diaminobenzidine (DAB) substrate, which forms black precipitates, and processed with TEM to visualize the vesicles inside the retinal ECs. In the $Lrp5^{-/-}$ mice, the number of HRP-positive vesicles was significantly increased, by about twofold, compared with WT control eyes (Fig. 1, E and F), whereas the number of HRP-positive vesicles in the $Ndp^{y/-}$ mice was increased by about fivefold compared with control eyes (Fig. 1, E and F). These findings further support increased functional EC transcytosis in both $Lrp5^{-/-}$ and $Ndp^{y/-}$ retinas, when Wnt signaling is absent.

MFSD2A is down-regulated in *Lrp5*- and *Ndp*-deficient retinal vessels

Gene array data from our previous work and others found significant down-regulation of *Mfsd2a* in $Lrp5^{-/-}$ and $Ndp^{y/-}$ retinas when compared with their respective WT controls (*16*, *37*). Here, we found that the mRNA levels of *Mfsd2a* were consistently down-regulated in $Lrp5^{-/-}$ retinas from postnatal day (P) 5 to P17, compared with age-matched WT controls (Fig. 2A). In addition, *Mfsd2a* levels were markedly decreased in P12 and P17 $Ndp^{y/-}$ retinas in comparison to littermate $Ndp^{y/+}$ controls (Fig. 2A). To further identify the cellular location of *Mfsd2a*, laser capture microdissection (LCM) was used to isolate blood vessels from retinal cross-sections, which were then analyzed for mRNA expression using reverse transcription quantitative polymerase chain reaction (RT-qPCR). In LCM-isolated retinal blood vessels, there was about a 10-fold enrichment of *Mfsd2a* in comparison to whole retinas in WT mice (Fig. 2B). Moreover, *Mfsd2a* mRNA levels were substantially down-regulated in both $Lrp5^{-/-}$ and $Ndp^{y/-}$ retinal vessels compared with their respective WT controls (Fig. 2C). Protein levels of MFSD2A were also significantly decreased in P17 $Lrp5^{-/-}$ and $Ndp^{y/-}$ retinas versus their respective WT control retinas by ~50% (Fig. 2D). In WT retinal flat mounts, immunochemistry staining of MFSD2A was observed almost exclusively in retinal blood vessels, showing colocalization with the vascular endothelium marker CD31, and was accentuated in microvessels (Fig. 2E). However, in both $Lrp5^{-/-}$ and $Ndp^{y/-}$ retinas, MFSD2A staining was

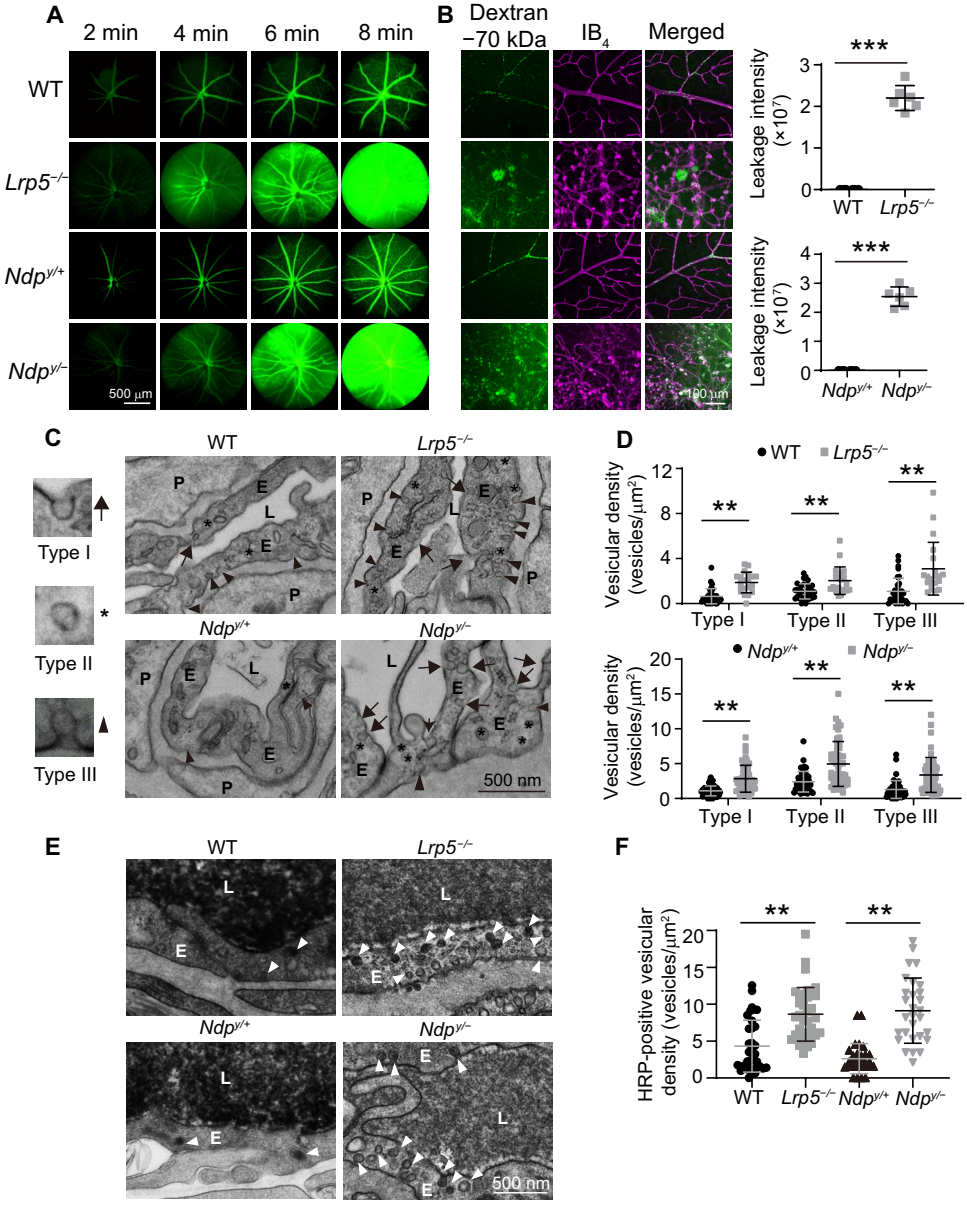

Fig. 1. *Lrp5*$^{-/-}$ and *Ndp*$^{y/-}$ mice have impaired BRB and increased number of transcytotic vesicles within their retinal vascular endothelium. (**A**) One-month-old *Lrp5*$^{-/-}$ and *Ndp*$^{y/-}$ and their control mice (WT and *Ndp*$^{y/+}$) were intraperitoneally injected with sodium fluorescein followed by fluorescent fundus imaging after 2, 4, 6, and 8 min. Green: Fluorescein within retinal blood vessels and extravasated fluorescein. (**B**) FITC-conjugated 70-kDa dextran (green) was injected retro-orbitally into *Lrp5*$^{-/-}$, *Ndp*$^{y/-}$, and control mice at P17. Isolated retinas were stained with IB_4 (magenta), with *Lrp5*$^{-/-}$ and *Ndp*$^{y/-}$ retinas showing pathological glomeruloid vascular structures. Vascular leakage was quantified by leakage intensity of extravasated FITC-conjugated dextran. (**C**) TEM images show transcytotic vesicles in the retinal vessel endothelium of 3-month-old *Lrp5*$^{-/-}$ and *Ndp*$^{y/-}$ mice and their controls. Left: Transcytotic vesicles are categorized into three types: luminal (arrows) or abluminal (arrowheads) membrane-connected and cytoplasmic vesicles (asterisks). E, endothelial cell; L, lumen; P, pericyte. (**D**) Quantification of transcytotic vesicular density in EM images, normalized by EC area. (**E** and **F**) HRP was retro-orbitally injected to *Lrp5*$^{-/-}$ (2 months old) and *Ndp*$^{y/-}$ mice (3 months old) and their age-matched controls, followed by TEM. The blood vessel lumen in HRP-injected mice was filled with electron-dense DAB reaction (black). HRP-filled vesicles (white arrowheads) were observed in retinal ECs and quantified (normalized by EC area). Scale bars, 500 μm (A), 100 μm (B), and 500 nm (C and D). Data are expressed as individual values plus means ± SD. $n = 3$ to 6 mice per group. Statistical differences between groups were analyzed using two-tailed unpaired *t* tests. $^{**}P < 0.01$, $^{***}P < 0.001$.

barely visible (Fig. 2E), further confirming its down-regulation in the absence of EC Wnt signaling.

Wnt signaling directly regulates MFSD2A transcription

We next assessed whether modulation of Wnt signaling directly regulates MFSD2A expression in human retinal microvascular ECs (HRMECs). *MFSD2A* mRNA levels were induced in HRMECs by a Wnt signaling activator, lithium, in a dose- and time-dependent manner (Fig. 3, A and B). Exposure to Wnt3a-conditioned medium also increased both the mRNA and protein levels of MFSD2A, whereas subsequent treatment with the Wnt inhibitor XAV939 reversed the Wnt-induced MFSD2A up-regulation in HRMECs

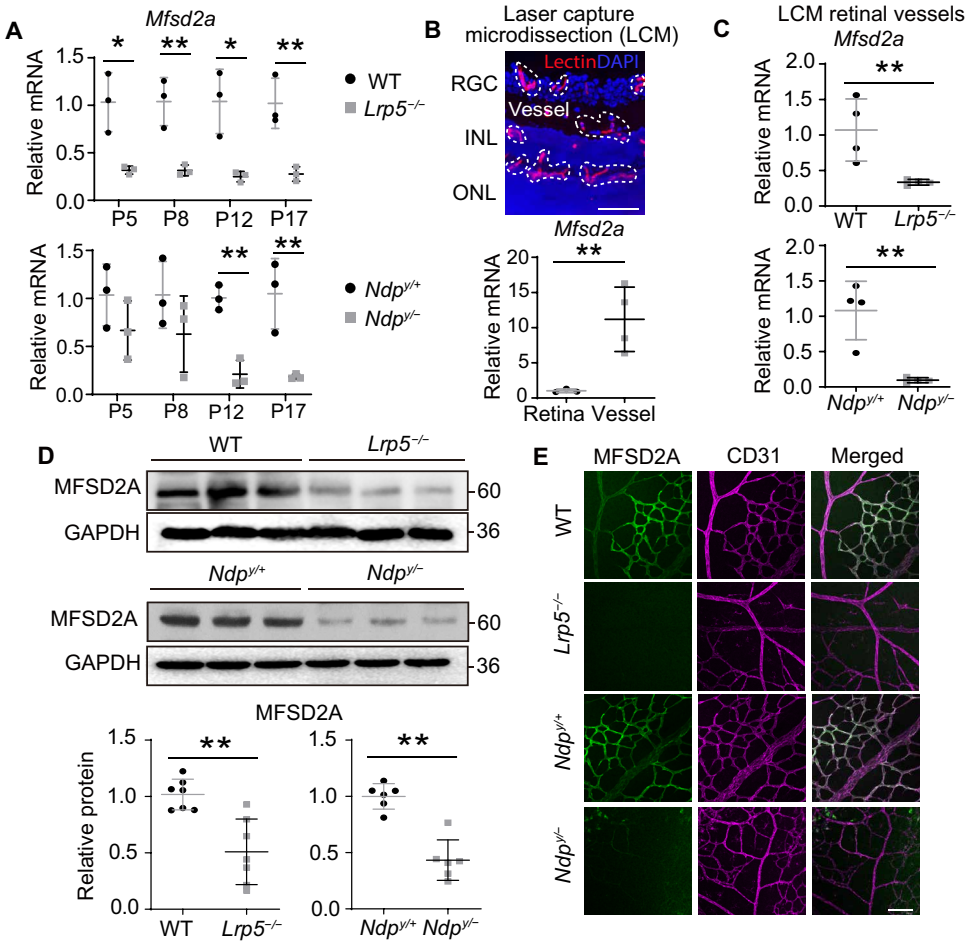

Fig. 2. MFSD2A levels are down-regulated in the retinas of Wnt signaling–deficient mice. (**A**) mRNA levels of *Mfsd2a* were measured by RT-qPCR in *Lrp5*$^{-/-}$ and *Ndp*$^{y/-}$ retinas and their respective controls at P5, P8, P12, and P17. (**B** and **C**) Laser-captured microdissection (LCM) was used to isolate retinal blood vessels (red), outlined by the white dashed lines in (C) illustrating retinal cross-sections (left). Cell nuclei were stained with 4′,6-diamidino-2-phenylindole (DAPI) (blue). RGC, retinal ganglion cells; INL, inner nuclear layer; ONL, outer nuclear layer. (B) Enrichment of *Mfsd2a* mRNA levels in LCM isolated blood vessels compared with the whole retina. (C) Comparisons of *Mfsd2a* mRNA levels in the retinal vessels of *Lrp5*$^{-/-}$/*Ndp*$^{y/-}$ mice with their controls. (**D**) Protein levels of MFSD2A in *Lrp5*$^{-/-}$ and *Ndp*$^{y/-}$ retinas were quantified and normalized by glyceraldehyde-3-phosphate dehydrogenase (GAPDH) levels. (**E**) Retinas were costained with MFSD2A and CD31, which colocalize in the WT eyes. MFSD2A staining is barely visible in *Lrp5*$^{-/-}$ and *Ndp*$^{y/-}$ retinas. Scale bars, 50 μm (B) and 100 μm (E). Data are expressed as individual values plus means ± SD. $n = 3$ to 6 per group. Statistical differences between groups were analyzed using two-tailed unpaired *t* tests. $^{*}P < 0.05$, $^{**}P < 0.01$.

(Fig. 3, C and D). XAV939 is a small-molecule inhibitor of the Wnt signaling pathway, which blocks Wnt signaling through binding to tankyrase, thus resulting in the stabilization of the Axin proteins, and increased degradation of β-catenin (*38*). Effects on Wnt signaling by Wnt modulators were validated by the levels of the active β-catenin (nonphosphorylated β-catenin), the canonical Wnt effector (Fig. 3D).

Canonical Wnt signaling mediates its gene expression by acting through the β-catenin–responsive TCF-binding motifs (A/TA/TCAAAG) on regulatory regions of its target genes (*39*). To evaluate whether Wnt signaling directly regulates *MFSD2A* expression at the transcriptional level, dual-luciferase reporter assays were performed in human embryonic kidney (HEK) 293T cells. Three promoter regions containing the putative TCF-binding motifs upstream of *MFSD2A* gene were cloned and ligated with a luciferase reporter. The luciferase reporter–containing promoter region #1 (P1) (but not #2-P2 or #3-P3) showed a more than 10-fold increase in luciferase activity when cotransfected with active β-catenin (Fig. 3E). In addition, when the TCF-binding motif on P1 was mutated, its luciferase reporter activity was significantly decreased when cotransfected with active β-catenin (Fig. 3F). Together, these results suggest that Wnt signaling directly regulates MFSD2A transcription via β-catenin binding to its promoter region site.

Wnt signaling pathway regulates vascular EC transcytosis through MFSD2A

To explore whether Wnt signaling regulates transcytosis specifically in vascular ECs, we developed an HRP-based in vitro transcytosis assay using HRMECs cultured in Transwells. Transcytosis of HRP across the EC monolayer from the upper chamber to the lower chamber was measured after extensive washing to detect the release of endocytosed HRP, which excludes the potential contribution from paracellular transport (Fig. 3G). Up-regulation of Wnt signaling with treatment of either Wnt3a-conditioned medium (Fig. 3H) or

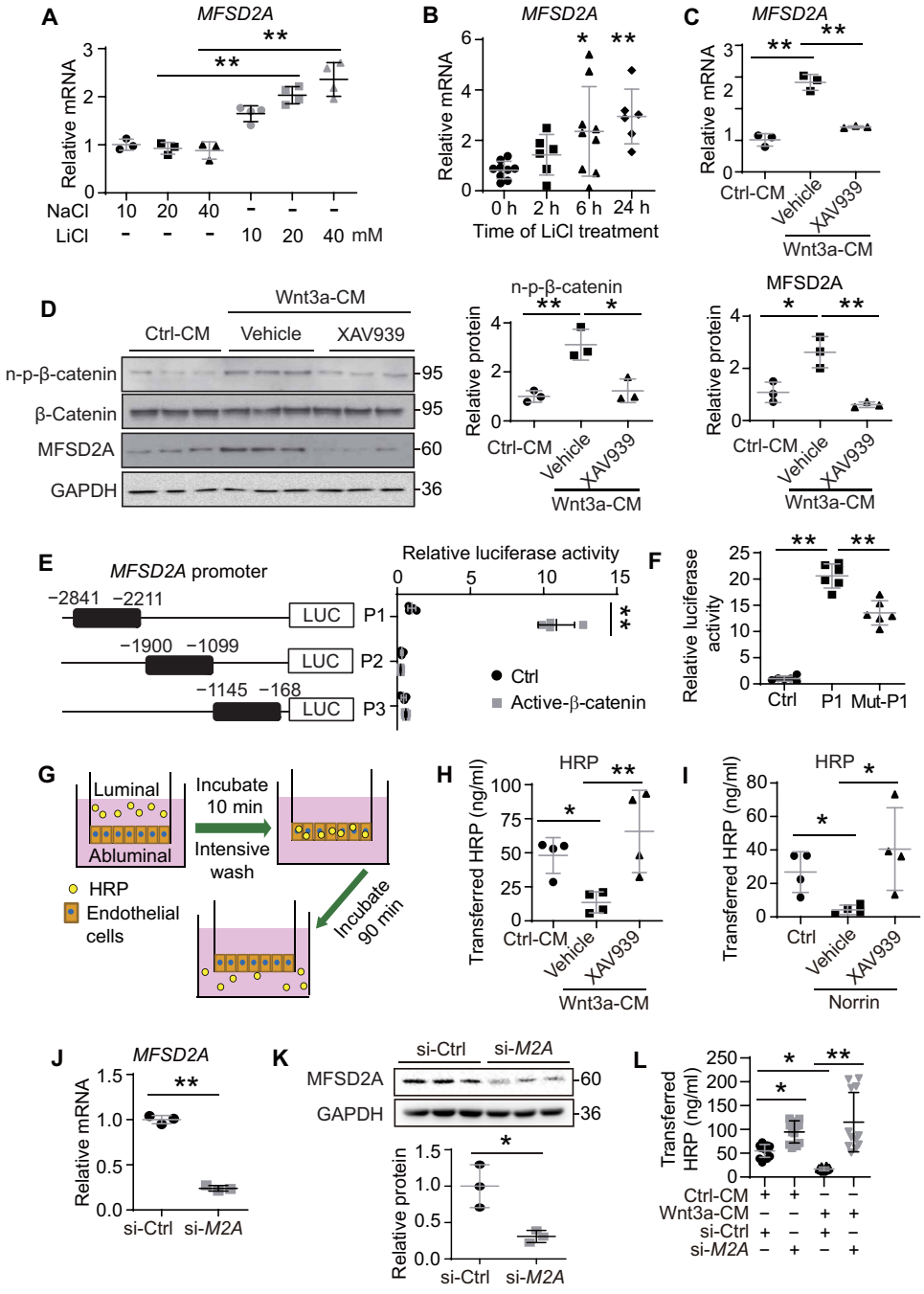

Fig. 3. Wnt signaling modulates endothelial transcytosis through its direct target gene MFSD2A. (**A** and **B**) *Mfsd2a* mRNA levels were increased in HRMEC treated with lithium chloride (LiCl), using control sodium chloride (NaCl). (**C** and **D**) *Mfsd2a* mRNA and protein levels were induced by Wnt3a-conditioned medium (Wnt3a-CM) and suppressed by the Wnt inhibitor XAV939. n-p-β-catenin, nonphosphorylated β-catenin. (**E**) Three promoter regions upstream of MFSD2A gene were identified containing putative Wnt-responsive TCF-binding motifs (TTCAAAG): P1 (−2841 to −2211 bp), P2 (−1900 to −1099 bp), and P3 (−1145 to −168 bp), followed by cloning and ligation with a luciferase reporter, and transfected with an active β-catenin plasmid in HEK293 cells. Luciferase activity was measured. (**F**) Mutation of TCF-binding site #1 (Mut-P1) (mutated to CCTGGGT) partially abolished the Wnt/β-catenin–responsive luciferase reporter activity compared with native P1. (**G**) Scheme of in vitro HRP transcytosis assay in ECs. (**H** and **I**) Transferred HRP in the lower chambers was measured to indicate the transcytosis levels through the EC monolayer. Activation of Wnt signaling activation was achieved by treatment with Wnt3a-CM (H) or human recombinant Norrin (I), and inhibition by XAV939 treatment. (**J** and **K**) siRNA targeting MFSD2A (si-*M2A*) suppressed MFSD2A mRNA (J) and protein levels (K) in HRMEC compared with si-control (si-Ctrl). (**L**) HRP-based in vitro transcytosis was used to detect transcytosis levels in HRMEC with Wnt3a-CM in combination with si-*M2A* or si-control (si-Ctrl) treatment (K). Data are expressed as individual values plus means ± SD. $n = 3$ to 4 per group. Statistical differences between groups were analyzed using a one-way analysis of variance (ANOVA) statistical test with Dunnett's multiple comparisons tests or two-tailed unpaired *t* tests. $^{*}P < 0.05$, $^{**}P < 0.01$.

recombinant Norrin (Fig. 3I) substantially reduced levels of EC transcytosis as measured by transferred HRP, whereas treatment with the Wnt signaling inhibitor XAV939 completely abolished the inhibitory effects of both Wnt3a and Norrin on EC transcytosis (Fig. 3, H and I). Together, these results suggest that the Wnt signaling pathway regulates transcytosis in ECs specifically.

Given the known role of MFSD2A in negatively regulating transcytosis (*7*, *40*), we next evaluated whether the effects of Wnt signaling on EC transcytosis were mediated by MFSD2A. In HRMECs, MFSD2A small interfering RNA (siRNA) treatment successfully suppressed the protein levels of MFSD2A by ~70% (Fig. 3J). While Wnt3a-conditioned medium in HRMEC inhibited EC transcytosis, MFSD2A siRNA significantly induced EC transcytosis in the control condition and also completely abolished the inhibitory effects of Wnt3a-conditioned medium in EC transcytosis (Fig. 3K). These results suggest that the inhibition of MFSD2A promotes EC transcytosis and reverses the Wnt-driven suppression of EC transcytosis.

Lrp5$^{-/-}$ and *Ndp*$^{y/-}$ retinal vascular endothelia have high levels of CAV-1 and caveolar vesicles

To further explore the types of vesicles involved in Wnt-mediated retinal EC transcytosis, we measured EC vesicles from *Lrp5*$^{-/-}$, *Ndp*$^{y/-}$, and their control retinas. All vesicles had a diameter range of 50 to 80 nm (fig. S1), in line with the diameter of normal caveolae, which are important for lipid raft–dependent and clathrin-independent endocytosis (*41*). Caveolin-1 (CAV-1) is a major component and marker of the caveolar vesicles (*42*). In *Lrp5*$^{-/-}$ and *Ndp*$^{y/-}$ retinas, both the mRNA and protein levels of CAV-1 were significantly increased (Fig. 4, A and B). However, clathrin, a marker for another major type of larger vesicle (~100 nm), remained unchanged in both *Lrp5*$^{-/-}$ and *Ndp*$^{y/-}$ retinas compared with their respective controls (Fig. 4A). These results pinpoint that caveolae-associated transcytosis is likely the main class of EC vesicles regulated by Wnt signaling. CAV-1 is highly colocalized with the endothelium marker IB_4 in *Lrp5*$^{-/-}$ and *Ndp*$^{y/-}$ and their control retinas (Fig. 4C). Moreover, immunogold labeling of CAV-1 in TEM showed a clear association of electron-dense gold particles, reflecting CAV-1 staining, with caveolar vesicles, and a substantial increase of CAV-1–positive transcytotic vesicles in *Ndp*$^{y/-}$ retinal vascular endothelia compared with their littermate WT controls (Fig. 4, D and E), suggesting that Wnt signaling regulates EC transcytosis via caveolae.

Overexpression of MFSD2A suppresses Wnt deficiency–induced transcytosis through CAV-1 and caveolar vesicles

To evaluate whether restoring MFSD2A levels may rescue the abnormally high levels of EC transcytosis in Wnt-deficient ECs, XAV939 was used to inhibit Wnt signaling in HRMECs, and MFSD2A overexpression (with FLAG tag) was achieved with lentiviral delivery, which was validated with a more than twofold protein overexpression (Fig. 5, A and B). Wnt inhibition induced CAV-1 protein levels by more than twofold, which was reversed by MFSD2A overexpression (Fig. 5, A and B). Active β-catenin levels were consistently low with Wnt inhibition, regardless of MFSD2A overexpression (Fig. 5, A and B). Moreover, MFSD2A overexpression completely abolished the functional effects of the Wnt inhibitor XAV939 on HRP-based EC transcytosis in vitro (Fig. 5C). These data suggest that regulation of EC CAV-1 levels and transcytosis by Wnt signaling is dependent on MFSD2A.

We next evaluated whether restoring MFSD2A levels in Wnt-deficient retinas may functionally restore the effects of Wnt signaling on limiting EC transcytosis. Lentiviruses expressing MFSD2A were intravitreally injected into *Lrp5*$^{-/-}$ retinas, which showed a more than threefold increase in the levels of MFSD2A protein in vivo (Fig. 5, D and E). MFSD2A overexpression also significantly suppressed CAV-1 protein levels in *Lrp5*$^{-/-}$ retinas (Fig. 5, D and E). Moreover, TEM imaging analysis showed that retinal overexpression of MFSD2A substantially decreased the number of transcytotic vesicles (both type I and type II) in the vascular endothelium of *Lrp5*$^{-/-}$ retinas (Fig. 5F). Consistently, the levels of immunogold CAV-1–positive transcytotic vesicles in *Lrp5*$^{-/-}$ retinas were also substantially decreased by the overexpression of MFSD2A (Fig. 5G). Together, these findings suggest that overexpression of MFSD2A restores the effects of Wnt signaling on limiting vascular EC transcytosis and EC caveolar vesicles in vivo.

Altered omega-3 fatty acid lipid profile in *Lrp5*$^{-/-}$ and *Ndp*$^{y/-}$ retinas is consistent with the basic role of MFSD2A as a lipid transporter

In addition to inhibiting transcytosis, a major role of MFSD2A is a lipid transporter in mediating the transport of DHA, an omega-3 long-chain polyunsaturated fatty acid essential for the development and function of the brain and retina (*33*, *43*). Fatty acid analysis was performed in the retinas and brains of *Lrp5*$^{-/-}$ and *Ndp*$^{y/-}$ mice and their littermate controls to compare the lipid profiles that might be influenced by the down-regulation of MFSD2A. DHA (22:6n3) and eicosapentaenoic acid (EPA, 20:5n3) were both significantly decreased in *Lrp5*$^{-/-}$ and *Ndp*$^{y/-}$ retinas compared with their relative control retinas (Fig. 6A). No significant changes were detected in other analyzed fatty acids (fig. S2). Because MFSD2A only transports fatty acids in the form of esters with lysophosphatidylcholines and prefers to transport long-chain fatty acids across the CNS barrier (*33*), down-regulation of DHA and EPA in the Wnt signaling–deficient retinas is very likely related to the suppression of MFSD2A. DHA and EPA levels in the *Lrp5*$^{-/-}$ and *Ndp*$^{y/-}$ brains, however, remain unchanged in comparison to their controls (Fig. 6B), which is consistent with their comparable brain sizes and brain weights (fig. S3), and this result may reflect alternate lipid transport mechanisms in the brain.

DISCUSSION

Our findings establish that the Wnt signaling pathway is an important regulator of retinal EC transcytosis and BRB integrity, in part through its modulation of MFSD2A, which has dual function of inhibiting transcytosis and transporting lipids. Using two animal models, *Lrp5*$^{-/-}$ and *Ndp*$^{y/-}$ mice, we demonstrated that Wnt signaling–deficient mice have abnormally increased levels of vascular EC transcytosis in the inner BRB. Wnt signaling limits EC transcytosis through direct transcriptional activation of MFSD2A, which largely suppresses the CAV-1–dependent caveolar transcytosis in the BRB (Fig. 6C).

Our work suggests that a Wnt signaling deficiency in the retina leads to increased EC transcytosis, thereby contributing, in part, to impaired BRB development and retinal vascular leakage. The barriers of CNS require specialized characteristics to maintain its integrity, including tight junctions and normally very low rates of transcytosis (*44*). Previous studies revealed that genetic deletion of either Norrin

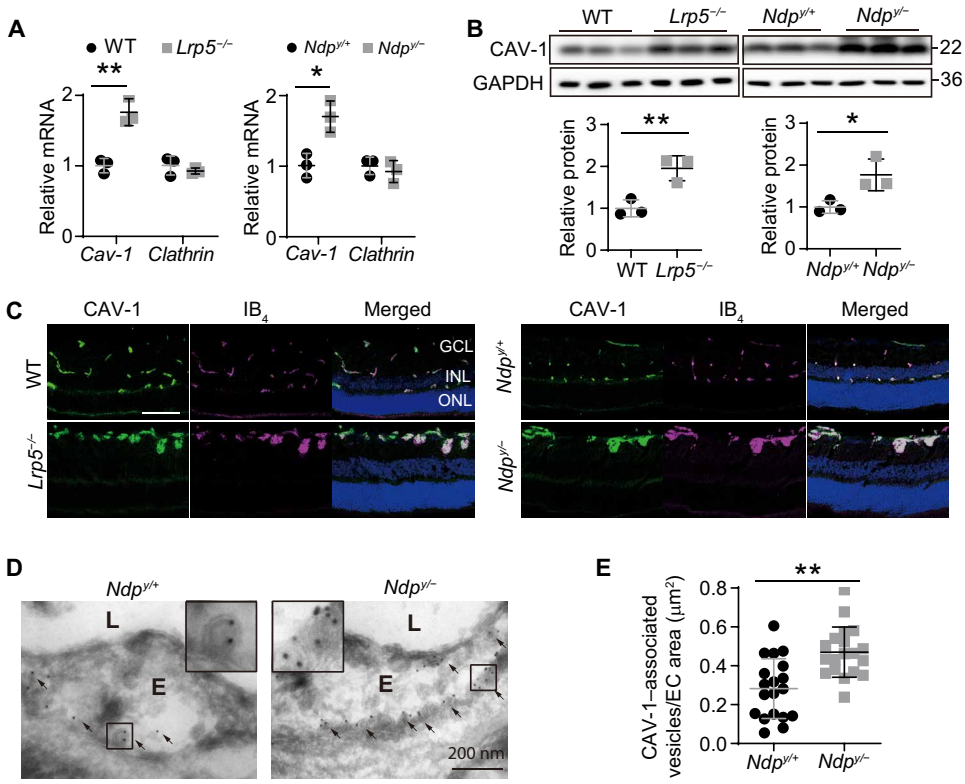

Fig. 4. CAV-1 levels and CAV-1–associated transcytosis are increased in Wnt-deficient retinas. (**A**) mRNA levels of *Cav-1* and *Clathrin* were measured in the retinas of $Lrp5^{-/-}$ and $Ndp^{y/-}$ mice and compared with their respective controls. (**B**) The protein levels of CAV-1 were detected by Western blot in the retinas of $Lrp5^{-/-}$ and $Ndp^{y/-}$ mice compared with their respective controls. (**C**) CAV-1) and IB_4 costaining in $Lrp5^{-/-}$ and $Ndp^{y/-}$ and their respective control retinas at P17. CAV-1 (green) and IB_4 (magenta) staining colocalize in the retina. Scale bar, 50 μm. GCL, ganglion cell layer. (**D** and **E**) CAV-1 was labeled with immunogold and imaged with electron microscopy (black dots, D). Scale bar, 200 nm. The numbers of Cav-1 associated vesicles were counted and normalized by EC area (E). Data are expressed as individual values plus means ± SD. $n = 3$ to 6 per group. Statistical differences between groups were analyzed using two-tailed unpaired *t* tests. $^*P < 0.05$, $^{**}P < 0.01$.

or co-receptor LRP5 led to decreased expression of the tight junction protein claudin 5 and increased expression of the fenestration marker PLVAP, thereby partially contributing to increased retinal vascular permeability due to loosened paracellular transport (*16*). Our TEM images show that tight junctions were absent in the retinal endothelium of both $Lrp5^{-/-}$ and $Ndp^{y/-}$ mice, which also exhibit fenestration (fig. S4), in line with findings from previous studies (*16*, *45*, *46*). Yet, until recently, the importance of a low transcytosis rate in maintaining a healthy BBB or BRB has been understudied. In 2014, Ben-Zvi *et al.* (*7*) compared gene expression patterns in ECs isolated from the brain cortex and the lungs and identified MFSD2A as a transmembrane protein that regulates BBB formation by suppressing transcytosis. Later, the same group found that the BBB and BRB of $Mfsd2a^{-/-}$ mice were surprisingly leaky, even with perfectly functional tight junctions, thereby leading to the conclusion that the vascular leakage in $Mfsd2a^{-/-}$ mice resulted from increased transcytosis (*7*, *40*). Yet controversy also exists, as two later studies using $Mfsd2a^{-/-}$ mice of different strains or background did not observe increased transcytosis in their retina and brains (*47*, *48*). Whether these different findings and the discrepancies may result from the different strains or genetic background of the $Mfsd2a^{-/-}$ mice awaits further investigation.

In this study, we observed a severe BRB breakdown phenotype in both $Lrp5^{-/-}$ and $Ndp^{y/-}$ mice (Fig. 1). Our data show that the BRB breakdown is induced by abnormally high levels of EC transcytosis, which were negatively regulated by the Wnt signaling pathway in the BRB and retinal ECs. Our data suggest that under normal conditions, Wnt signaling limits EC transcytosis to help maintain BRB integrity. However, when Wnt signaling is deficient under pathological conditions, our findings show that EC transcytosis becomes unchecked, leading to enhanced vascular leakage. This work demonstrates that Wnt signaling serves as a key controlling mechanism of EC transcytosis in vascular endothelial barrier structures, in addition to paracellular transportation regulation through tight junctions.

We found that Wnt signaling regulation of transcytosis is mediated by direct transcriptional regulation of the Wnt target gene MFSD2A, which is enriched in the vascular endothelium. Gene array data from our previous studies and others found that the expression levels of *Mfsd2* in the retinas of both $Lrp5^{-/-}$ and $Ndp^{y/-}$ mice were substantially down-regulated compared with their respective WT controls (*16*, *37*). Here, we found that MFSD2A levels are specifically down-regulated in $Lrp5^{-/-}$ and $Ndp^{y/-}$ retinal vessels versus their respective WT controls. Our findings show that Wnt signaling positively regulates MFSD2A expression on a transcriptional level, and MFSD2A is a direct target gene of the Wnt/β-catenin signaling pathway as confirmed by luciferase assay. These findings are in line with a recent study showing that elevated β-catenin signaling leads to a partial conversion of permeable CNS ECs to a barrier-type state through the up-regulation of not only tight junction proteins

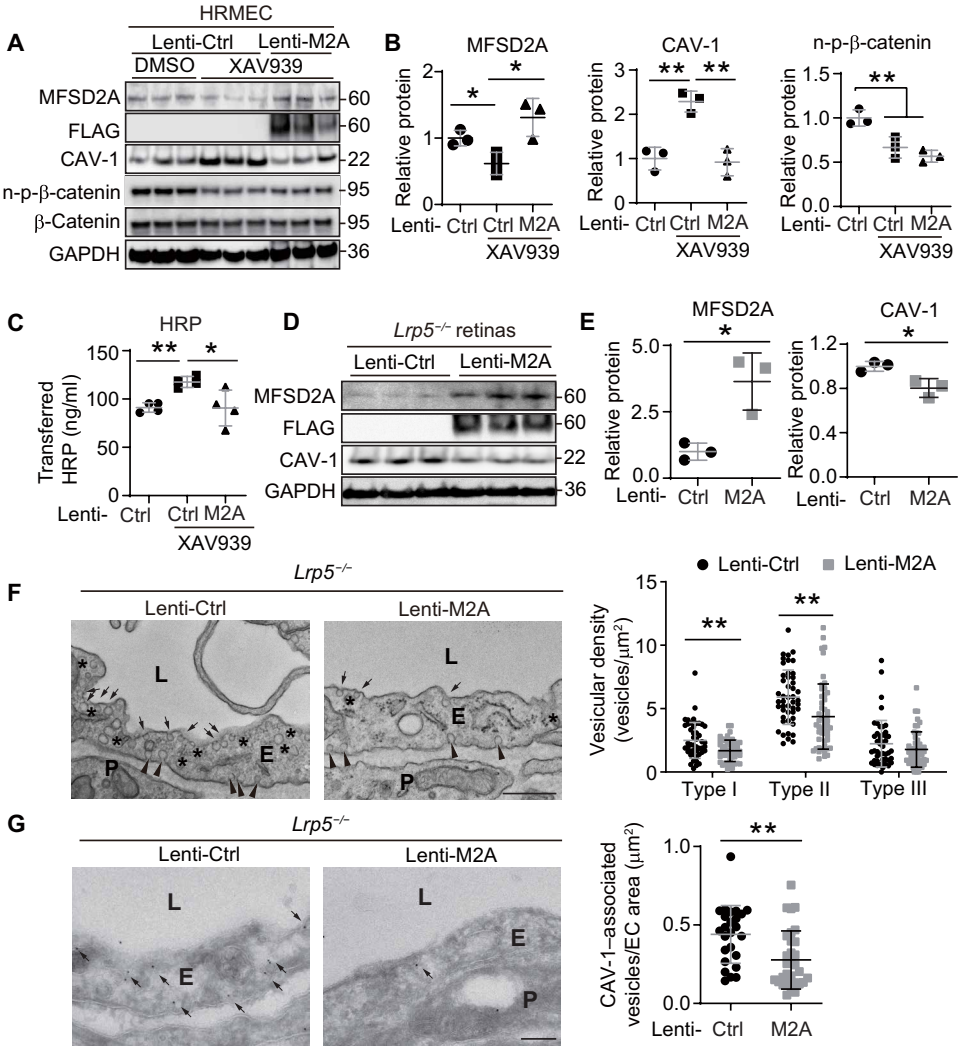

Fig. 5. Lentivirus overexpressing MFSD2A inhibits Wnt deficiency–induced up-regulation of caveolar transcytosis. (**A** to **C**) HRMECs were treated with XAV939 to inhibit Wnt signaling and infected with Lenti-M2A to detect the effect of MFSD2A overexpression on Wnt signaling–induced up-regulation of CAV-1. (A) Protein levels were shown with Western blot. (B) Relative protein levels of nonphosphorylated β-catenin (n-p-β-catenin), MFSD2A, and CAV-1 were normalized by GAPDH. (C) Inhibition of Wnt signaling by XAV939 induced an increase of transferred HRP, while overexpression of MFSD2A reversed the changes. (**D** to **G**) Lenti-M2A and its control were injected intravitreally into *Lrp5*$^{-/-}$ mice at P10. Mice were euthanized at P30. (D) Retinas were used to detect protein levels with Western blot. (E) Quantification of relative protein levels of MFSD2A and Cav-1 in lenti-M2A– and lenti-control–treated *Lrp5*$^{-/-}$ retinas, normalized by GAPDH. (F) Fixed *Lrp5*$^{-/-}$ retinas with lenti-M2A and lenti-control treatment were prepared for electron microscopy analysis. Transcytotic vesicles in the retinal vessel endothelia of *Lrp5*$^{-/-}$ mice were categorized into three groups (representative images of three groups were shown in Fig. 1). Overexpression of MFSD2A by lentivirus decreased the transcytotic vesicles of type I (arrows) and type II (asterisks), but not type III (arrowheads). (G) CAV-1 was labeled with immunogold in *Lrp5*$^{-/-}$ retinas treated with lenti-M2A and lenti-control, and immunogold was detected with electron microscopy (black dots). The numbers of CAV-1–associated vesicles were counted and normalized by EC area. Scale bars, 500 nm (F) and 200 nm (G). Data are expressed as individual values plus means ± SD. $n = 3$ per group. Statistical differences between groups were analyzed using an ANOVA statistical test with Dunnett's multiple comparisons tests or two-tailed unpaired *t* tests. *$P < 0.05$, **$P < 0.01$.

such as claudin5 but also gene transcription of MFSD2A (*49*). Because *Lrp5*$^{-/-}$ and *Ndp*$^{y/-}$ retinas show elevated levels of vascular endothelial growth factor (VEGF) as a secondary result of the hypoxic retina environment (*50*, *51*) (fig. S5A), and VEGF is a key vascular permeability regulator capable of regulating several tight junction proteins and also a known downstream target of Wnt signaling, there is a question whether increased VEGF levels in *Lrp5*$^{-/-}$, *Ndp*$^{y/-}$, and their control retinas may also contribute to the regulation of *MFSD2A* expression. We found that recombinant VEGF treatment does not alter *MFSD2A* expression in HRMECs, compared with control (fig. S5), indicating that VEGF does not directly regulate *MFSD2A* expression, and that *MFSD2A* activation in *Lrp5*$^{-/-}$ and *Ndp*$^{y/-}$ mice is VEGF independent and directly resulted from Wnt deficiency. Our concept that Wnt signaling regulation of transcytosis is mediated through MFSD2A is further supported by experiments knocking down MFSD2A in retinal ECs, which reversed the suppression of transcytosis by Wnt signaling. In addition, overexpression of MFSD2A in *Lrp5*$^{-/-}$ retinas restored transcytosis levels in retinal

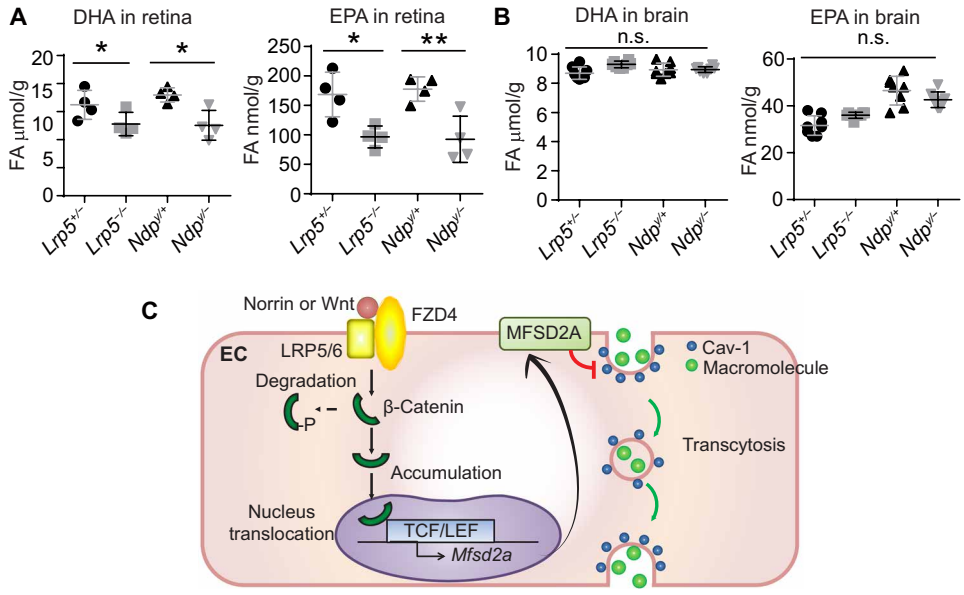

Fig. 6. Fatty acid DHA and EPA levels are decreased in the retinas of Wnt signaling–deficient mice. (**A** and **B**) Long-chain polyunsaturated fatty acids in the retina or brain were measured. Both DHA and EPA were down-regulated in the retinas of *Lrp5*$^{-/-}$ and *Ndp*$^{y/-}$ mice compared with their respective controls (A), but remained unchanged in the brains of the same mice (B). Data are expressed as individual values plus means ± SD. $n = 4$ per group. Statistical differences between groups were analyzed using two-tailed unpaired *t* tests. *$P < 0.05$, **$P < 0.01$. n.s., not significant. (**C**) Scheme illustration on the role of Wnt signaling in controlling inner BRB integrity by limiting MFSD2A-mediated EC caveolar transcytosis. Canonical Wnt signaling is activated by binding of the ligand (Norrin or Wnts) to the receptor complex containing Frizzled4 (FZD4) and co-receptors (LRP5 or LRP6), leading to the prevention of β-catenin ubiquitination and degradation. Stabilized β-catenin then translocates to the nucleus and works with TCF to bind the TCF-responsive motif in the promoter region of MFSD2A, directly regulating its gene transcription. MFSD2A protein is located on cellular plasma membrane to suppress CAV-1 protein levels and block the formation of CAV-1–positive caveolae, thereby limiting EC transcytosis and maintaining inner BRB integrity.

endothelium back to normal levels as observed in WT, without affecting the impaired tight junctions in *Lrp5*$^{-/-}$ retinas (fig. S6). Together, these findings reveal that Wnt signaling is a previously unknown upstream regulator and direct transcriptional mediator of MFSD2A, down-regulation of which contributes to increased transcytosis in Wnt signaling–deficient retinas.

Our data suggest that Wnt signaling–mediated MFSD2A-dependent regulation of transcytosis in the BRB is primarily through the caveola-mediated pathway. Transcytotic pathways in epithelial cells and ECs can be categorized into clathrin-mediated, caveola-mediated, and other pathways (*52*). Clathrin-mediated vesicle trafficking (such as the transferrin receptor–mediated transcytosis of iron) is the most common pathway (*53*). Among many non–clathrin-mediated vesicle trafficking pathways, caveolae-mediated vesicle trafficking predominates as a transcytotic route in the ECs of peripheral organs, such as the heart and the lung (*54*, *55*). Previous research has also shown that the suppression of caveolae-mediated transcytosis is essential for BBB function and is mediated, in part, by MFSD2A (*35*). In addition, the lipids transported by MFSD2A mediate the suppression of caveolae transcytosis (*35*). In our study, the size of the vesicles observed in TEM images ranged from 50 nm to 80 nm (fig. S1), which fell into the diameter range of caveolae (*41*). The up-regulated caveolae marker CAV-1 was also found in the retinal ECs of *Lrp5*$^{-/-}$ and *Ndp*$^{y/-}$ mice. In addition, overexpression of MFSD2A diminished the increased CAV-1 in vitro in HRMECs and in *Lrp5*$^{-/-}$ retinas. Together, these findings suggest that Wnt signaling regulation of transcytosis in the BRB is primarily through the MFSD2A-dependent caveola-mediated pathway.

The fundamental function of MFSD2A is to act as a key transporter for DHA (*33*, *43*). Nguyen *et al.* (*33*) found that *Mfsd2a*$^{-/-}$ mice show significantly reduced levels of DHA in brain, which is associated with neuronal cell loss in the hippocampus and cerebellum, neurological and behavioral deficits, and reduced brain size. In addition, MFSD2A-assisted DHA transport is important for photoreceptor cell development in the eye, where MFSD2A deficiency leads to an approximately 50% reduction in retinal DHA (*47*, *48*). These findings are in line with our observation of a 20 to 30% reduction of retinal DHA with partial suppression (~50%) of MFSD2A in *Lrp5*$^{-/-}$ and *Ndp*$^{y/-}$ retinas. Our fatty acid analysis also found a significant decrease of both DHA (22:6n-3) and EPA (20:5n-3) in *Lrp5*$^{-/-}$ and *Ndp*$^{y/-}$ retinas but intriguingly not in their brains, suggesting a previously unidentified role of Wnt signaling in mediating essential fatty acid transportation via MFSD2A in the retina. The reasons underlying the different fatty acid profiles between brain and retina tissue in Wnt signaling–deficient mice still need further investigation, but may be a reflection of the cellular structural differences in retina versus brain, as well as the differential presence of other redundant lipid transport mechanisms (*56*) or differential mechanisms related to MFSD2A stability and function. For example, the Zika virus was recently shown to be capable of disrupting MFSD2A and promoting its ubiquitination and degradation to impair MFSD2A-mediated DHA uptake in the brain (*57*). The transportation function of MFSD2A relates to its transcytosis regulatory function. Lipids (mainly DHA) transported by MFSD2A create a unique lipid composition within CNS ECs that specifically inhibit caveola-mediated transcytosis to maintain BBB integrity (*35*). In our study, the significant

reduction of DHA levels in the retinas of $Lrp5^{-/-}$ and $Ndp^{y/-}$ mice may also contribute to the up-regulation of caveola-mediated transcytosis in the BRB.

Maintaining a healthy BRB is crucial for retinal function (*9*, *10*, *14*, *15*). Our work provides a previously unexplored perspective with which to understand and target the caveolae vesicular route of transcytosis to protect the BRB, especially through one of the most fundamental signaling pathways, the Wnt signaling pathway (Fig. 6C). Considering that MFSD2A could serve as a therapeutic target for regulating transcytotic mechanisms in CNS ECs (*58*), our study may shed light on the development of new therapeutic strategies in Wnt signaling–related eye diseases. Furthermore, transcytosis often serves as a key route for drug delivery in the CNS (*59*). The barriers in the brain and retina, while maintaining an immune-exempted environment, sometimes also become obstacles for drug delivery to desired sites when treating neuronal diseases. Better ways to modulate transcytosis may assist in the selective delivery of medicine to the CNS tissue. Findings from this study can further our understanding of basic transcytosis regulation and may provide a feasible direction for treating retinal vascular leakage diseases and developing drug delivery systems.

MATERIALS AND METHODS

Experimental design

Mice with mutations of the Wnt signaling pathway components ($Lrp5^{-/-}$ and $Ndp^{y/-}$) were used to study the effects of Wnt signaling on vascular endothelial transcytosis in the BRB. FFA, in vivo BRB permeability assay, and TEM were used to analyze BRB integrity and vascular leakage in retinas. In vitro transcytosis assays were performed in HRMECs to evaluate direct modulation of Wnt signaling on transcytosis. The regulatory effects of Wnt signaling on the expression of MFSD2A were evaluated with real-time qPCR, Western blot, and dual-luciferase reporter assay. Lentiviruses expressing MFSD2A were generated to determine the effects of MFSD2A overexpression on Wnt-mediated EC transcytosis in vitro and in vivo. The CAV-1–associated caveolae pathway was assessed for the mechanisms of the Wnt/MFSD2A pathway in endothelial transcytosis. Fatty acids in both retinas and brains were measured to evaluate altered lipid profile in the absence of Wnt signaling.

Animal models and cell lines

$Lrp5^{-/-}$ (stock no. 005823) and its WT controls C57BL/6J (stock no. 000664) and $Ndp^{y/-}$ (stock no. 012287) were obtained from the Jackson Laboratory (Bar Harbor, ME). Male $Ndp^{y/+}$ mice were used as $Ndp^{y/-}$ controls because *Ndp* gene is X-linked. All experiments were approved by the Institutional Animal Care and Use Committee (IACUC) at Boston Children's Hospital and followed the guidelines within the Association for Research in Vision and Ophthalmology Statement for the Use of Animals in Ophthalmic and Vision Research. All experiments were performed with age-matched controls and with littermate controls when feasible.

Cells were maintained at 37°C with 5% CO_2. HRMECs were obtained from the Cell Systems Corporation (Kirkland, WA; ACBRI181) and cultured with the EGM-2 EC growth medium (Lonza, Portsmouth, NH). HEK293T cells (293T or HEK293T) were obtained from the American Type Culture Collection (ATCC) (Manassas, VA; CRL-3216) and cultured in high-glucose Dulbecco's modified Eagle's medium (DMEM) and 10% fetal bovine serum (FBS) (Thermo Fisher Scientific, Waltham, MA). L Wnt-3A cells (CRL-2647) and L cells (CRL-2648) for producing Wnt3a-conditioned medium and the control-conditioned medium were obtained from ATCC and cultured in high-glucose DMEM and 10% FBS.

Experimental model and subject details

Fundus fluorescein angiography

Mice were anesthetized with a mixture of xylazine (6 mg/kg) and ketamine (100 mg/kg), and pupils were dilated with topical drops of Cyclomydril (Alcon Laboratories, Fort Worth, TX). Fluorescein AK-FLUOR solution (Akorn, Lake Forest, IL; NDC17478-253-10) was intraperitoneally injected at 5 μg/g body weight into the anesthetized mice. Fluorescent fundus images were taken with the retinal imaging microscope (Micron IV, Phoenix Research Laboratories, Pleasanton, CA) at 2, 4, 6, and 8 min after fluorescein injection.

In vivo BRB permeability assay

FITC-conjugated dextran (70 kDa, 0.1 mg/g; Thermo Fisher Scientific; D1822) was injected retro-orbitally and allowed to circulate for 1 hour. Mice were then euthanized, and eyes were enucleated. Eyes were lightly fixed with 4% paraformaldehyde (PFA) for 15 min at room temperature, and retinas were dissected and flat-mounted. Whole-mounted retinas were imaged using confocal microscopy (LSM 880; Zeiss, Oberkochen, Germany). The fluorescence intensity of FITC-dextran was analyzed with Zeiss microscope software ZEN Intellesis to segment and quantify vascular leakage from retinal vessels based on previous protocols (*60*). Retinas were costained with Alexa Fluor 594–conjugated isolectin GS-IB_4 (Thermo Fisher Scientific; I21413).

Transmission electron microscopy

HRP (0.5 mg/g; Sigma-Aldrich, Natick, MA; P8250) was dissolved in phosphate-buffered saline (PBS) and injected retro-orbitally. After 1 hour of HRP circulation, eyes were enucleated and fixed in 4% PFA and 5% glutaraldehyde solution for 1 hour, followed by 4% PFA fixation overnight. Retinas were then dissected and cut into 50-μm-thick free-floating sections using a vibrotome. Sections were incubated for 45 min at room temperature in 0.05 M tris-HCl (pH 7.6) buffer containing DAB (0.5 mg/ml) (Sigma-Aldrich) with 0.01% hydrogen peroxide. Eyes without HRP injection were collected directly after the euthanasia of the mice, fixed, and cut in the same protocol without DAB staining. Sections were then stained with osmication and uranyl acetate, dehydrated in alcohols, and embedded in Taab 812 Epoxy Resin (Marivac Ltd., Nova Scotia, Canada). Sections (80 nm) were cut with a Leica ultracut microtome, picked up on 100-mesh formvar/carbon-coated copper grids, stained with 0.2% lead citrate, and viewed and imaged under the Philips Tecnai G2 Spirit BioTwin Electron Microscope or the JEOL 1200Ex Electron Microscope.

Immunogold labeling for electron microscopy

Mice were perfused with 4% PFA and 0.1% glutaraldehyde solution shortly after sacrifice. Eyes were collected and immersed in 4% PFA for postfixation overnight. Retinas were then dissected and infiltrated with 2.3 M sucrose in PBS before freezing in liquid nitrogen. Frozen samples were sectioned at −120°C, and the 80-nm sections were transferred to formvar/carbon-coated copper grids. Grids were stained with CAV-1 antibody (1:10; Cell Signaling Technology, Danvers, MA; 3267) for 30 min at room temperature, and Protein-A gold (10 nm, 1:50; University Medical Center, Utrecht, The Netherlands) for 20 min. Contrasting/embedding of the labeled grids was carried out on ice in 0.3% uranyl acetate in 2%

methylcellulose for 10 min. The grids were examined in a JEOL 1200EX or a Philips Tecnai G2 Spirit BioTwin TEM, and images were recorded with an AMT 2k charge-coupled device camera.

In vitro Transwell transcytosis assay

HRMECs were seeded on the inner surface of gelatin-coated Transwell inserts (6.5-mm-diameter, 0.4–μm–pore size polycarbonate filter; Corning, Corning, NY), which were then placed in wells of a 24-well plate with complete EGM2 medium. The culture medium was changed every other day. Transendothelial electrical resistance (TEER) was measured to assess the barrier function between confluent cells using an electrical resistance system (Millicell ERS-2, MilliporeSigma, Burlington, MA). When TEER reached 160 ohm·cm^2 (blank control is ~90 ohm·cm^2), usually 7 to 12 days after seeding, treatments were added to the upper chambers. Wnt3a-conditioned medium/control-conditioned medium (50% mixed with basic EBM2 medium), human recombinant Norrin (R&D Systems, Minneapolis, MN; 3014-NR), and XAV939 (10 μM, Selleckchem, Houston, TX; S1180) were added for 24-hour treatment. DsiRNA targeting human *MFSD2A* (Integrated DNA Technologies Inc.; pooled from hs.Ri.MFSD2A.13.1, hs.Ri.MFSD2A.13.2, and hs.Ri.MFSD2A.13.3)/Negative control DsiRNA (Integrated DNA Technologies Inc.; 51-01-14-03) or lentiviruses (production details below) were added for 72-hour treatment. Afterward, HRP (5 mg/ml) was added to the upper chambers and incubated at 37°C for 15 min. The Transwell plate was then placed on ice, and both the upper and lower chambers were intensively washed with P buffer for six times to remove all free extracellular HRP. Fresh EGM2 medium was then added to both the upper and lower chambers. Cells were incubated at 37°C for an additional 90 min before the medium from the lower chambers was collected. HRP levels in the lower chamber medium were reacted with QuantaBlu Fluorogenic Peroxidase Substrate (Thermo Fisher Scientific; 15169) and detected using a luminescence plate reader (EnSight Multimode Plate Reader, PerkinElmer, Akron, OH).

Laser capture microdissection

LCM was used to isolate blood vessels from retinal cross-sections of *Lrp5*$^{-/-}$, *Ndp*$^{y/-}$, or their respective WT control mice. Whole eyes were first isolated, embedded in optimal cutting temperature (OCT) compound, and then cryosectioned. Retinal cross-sections (10 μm thick) were then fixed briefly in ethanol and stained with Alexa Fluor 594–conjugated isolectin GS-IB$_4$. Samples were then transferred to a Leica LCM microscope (CTR 6500; Wetzlar, Germany), and lectin-positive blood vessels were microdissected using a laser. Samples were subsequently pooled for total RNA isolation and real-time qPCR.

Real-time qPCR

Total RNA was extracted using the PureLink RNA Mini Kit (Thermo Fisher Scientific; 12183025) from whole retina samples or HRMECs following treatment with lithium chloride, Wnt3a-conditioned medium, or the XAV939 Wnt signaling inhibitor. In addition, total RNA from LCM-isolated retinal vessels was extracted using the miRNeasy RNA Micro Kit (Thermo Fisher Scientific; 12183020). The PCR primers used in the experiments are the following: mouse *Mfsd2a*, 5′-AGAAGCAGCAACTGTCCATTT-3′ (forward) and 5′-CTCGGCCCACAAAAAGGATAAT-3′ (reverse); human *MFSD2A*, 5′-CCTTGTTTCCAGGACCTCAA-3′ (forward) and 5′-GAAGTAGGCGATTGGCTCAG-3′ (reverse); mouse *Cav-1*, 5′-GCATCAGCACGCAGAAAGAG-3′ (forward) and 5′-ACTTGGAATTGGCACCAAGGA-3′ (reverse); mouse *Clathrin*, 5′-ATTCTAGCCTCGCAGGATGC-3′ (forward) and 5′-ACCACACGATTTTGCTGTGC-3′ (reverse); mouse *Vegf*, 5′-ACTCGGATGCCGACACGGGA-3′ (forward) and 5′-TGCTCCCCGGCAGGCAAAAG-3′ (reverse); *18S*, 5′-ACGGAAGGGCACCACCAGGA-3′ (forward) and 5′-CACCACCACCCACGGAATCG-3′ (reverse). mRNA levels were quantified by normalizing the number of amplified complementary DNA (cDNA) copies to the housekeeping gene *18S* using the ΔΔ–C_T method.

Western blotting

Western blot analysis was used to measure the proteins of interest in retinas and HRMEC. Retina or cell samples were extracted and sonicated in radioimmunoprecipitation assay lysis buffer (Thermo Fisher Scientific; 89901) containing protease and phosphatase inhibitors (Sigma-Aldrich; P8465, P2850). Protein concentration was then measured with BCA protein assay kit and normalized across samples. Equal amounts of protein were subsequently loaded in NuPAGE bis-tris protein gels (Thermo Fisher Scientific) and transferred to a polyvinylidene difluoride membrane. Membranes were blocked with 5% nonfat milk for 1 hour and then incubated with a primary monoclonal antibody overnight at 4°C. Primary antibodies used were anti-MFSD2A (Abcam, Cambridge, MA; ab105399), anti–CAV-1 (Cell Signaling Technology, Beverly, MA; 3267), anti–nonphosphorylated β-catenin (Cell Signaling Technology; 8814S), anti–β-catenin (Santa Cruz Biotechnology, Santa Cruz, CA; sc-7199), anti-FLAG (Sigma-Aldrich; SAB4200071), anti-CD31/PECAM-1 (R&D Systems; AF3628), and anti–glyceraldehyde-3-phosphate dehydrogenase (GAPDH) (Santa Cruz Biotechnology, sc-32233). HRP-linked secondary antibodies (Sigma-Aldrich; anti-mouse antibody, NA9310; anti-rabbit antibody, SAB3700934) were applied at 1:5000 dilution. The enhanced chemiluminescence reagent (Thermo Fisher Scientific; 34075) was used as HRP substrate. Chemiluminescent signals were detected using an imaging system (17001401, Bio-Rad, Hercules, CA), and densitometry was analyzed using ImageJ software.

Retinal immunohistochemistry staining and flat mounting

Mice were sacrificed at P6. Eyeballs were enucleated and fixed with 4% PFA at room temperature for 20 min followed by a cold 70% ethanol fixation at −20°C overnight. Retinas were dissected and stained overnight at 4°C with primary antibodies including CD31 antibodies (1:500; R&D Systems; AF3628), MFSD2A antibodies (1:500; a gift from D. Silver at Duke-NUS Graduate Medical School, Singapore), and CAV-1 (Cell Signaling Technology, Danvers, MA; 3267). Retinas were then washed and stained with secondary antibodies including Alexa Fluor 488–conjugated chicken anti-rabbit (Thermo Fisher Scientific; A-21441) and Alexa Fluor 594–conjugated donkey anti-goat (Thermo Fisher Scientific; A-11058) at room temperature for 1 hour, followed by whole mounting and imaging with a confocal microscope (LSM 880, Zeiss).

Mfsd2a promoter cloning and dual-luciferase reporter assay

Three mouse *Mfsd2a* promoter regions containing the putative TCF-binding motif (A/TA/TCAAAG) were amplified by PCR using Phusion High-Fidelity DNA polymerase (New England Biolabs, Ipswich, MA; M0530). Primers used for cloning were the following: M2A_Promoter_1, 5′-TATCGCTAGCAGACCCAGAAAGGGGACTGG-3′ (forward) and 5′-TATCCTCGAGGCCCACGATTTTCTTCCACT-3′ (reverse); M2A_Promoter_2, 5′-TATCGCTAGCCTGACAGACTGGAATCGGGC-3′ (forward) and 5′-TATCCTCGAGCCGTCATCATCTAAACAGAGGC-3′ (reverse); M2A_Promoter_3, 5′-TATCGCTAGCCGTTCTCTGCTGGCACCTAT-3′ (forward) and 5′-TATCCTCGAGCTCCGCGCCTCTTAAAGGTT-3′ (reverse). The PCR products were then purified by gel extraction

and cloned into the destination pGL3 promoter luciferase vector (Promega, Madison, WI; E1751). All clones were verified by Eton Bioscience (Boston, MA) and confirmed by 100% sequence matching with the promoter region of *Mfsd2a*. The TCF-binding site (TTCAAAG, −2605 to −2599) in Promoter #1 (−2841 to −2211) was mutated to CCTGGGT using a QuikChange Lightning kit (Agilent Technologies, Lexington, MA; 210515). The primer pairs used for mutation were 5′-GTAGAAAGGAGAACTCCTGGGTGGACTA-ATGGAGTTAC-3′ (forward) and 5′-GTAACTCCATTAGTC-CACCCAGGAGTTCTCCTTTCTAC-3′ (reverse).

Promoter plasmids and an active form of β-catenin plasmid were transfected into HEK293T cells. After 48 hours, a dual-luciferase reporter assay kit (Promega; E1910) was used to determine luciferase activity. The relative luciferase activity was calculated by normalizing the firefly luciferase activity values to the respective *Renilla* luciferase values.

Lentivirus production and application

A plasmid expressing the full-length sequence of mouse *Mfsd2a* was optimized and synthesized by Synbio Technologies (Monmouth Junction, NJ). FLAG tag was added to the C terminus of MFSD2A protein for detection. Lentivirus vector pCDH-CMV-MCS-EF1-puro (SBI System Biosciences, Palo Alto, CA; CD510B-1) was used as the backbone. The sequence of green fluorescent protein (GFP) was constructed to the same backbone as a control. pRSV-Rev (Addgene, Watertown, MA; ID 12253), pMDLg/pRRE (Addgene; 12251), and pCMV-VSV-G (Addgene; 8454) were used as packaging plasmids. MFSD2A- or GFP-lentivirus plasmids and the packaging plasmids were transfected into HEK293T cells for 72 hours. Medium was collected and filtered through a 0.45–μm–pore size filter (Corning Life Sciences; 430768) to remove cell debris. The flow-through was then centrifuged with a speed of 20,000 rpm for 2 hours. The pellets were air-dried and resuspended with PBS.

For lentiviral transduction in HRMECs, 2-μl lentivirus and polybrene (final concentration, 8 μg/ml) were added to each well in six-well plates. Further experiments were performed after 72 hours of viral infection. For lentiviral transduction in mouse eyes, 0.5-μl lentivirus was injected intravitreally at P12, and mice were euthanized at P30 and their retinas were processed for protein expression detection or electron microscopy.

Fatty acid analysis

Littermate controls of $Lrp5^{-/-}$ and $Lrp5^{+/-}$, $Ndp^{y/-}$ and $Ndp^{y/+}$ were sacrificed at P17. Heterozygous $Lrp5^{+/-}$ mice are phenotypically normal (*16*) and were used as littermate controls for comparable maternal care and milk/diet. Retinas and brains (cortex) were isolated promptly and stored at −80°C until further processing. Retina and brain total lipids were extracted using chloroform, methanol, and 0.88% KCl (2:1:0.75 by volume). Total phospholipids were isolated by thin-layer chromatography (TLC) using TLC G-plates (EMD Chemical, Gibbstown, NJ) with authentic standards (Avanti, Alabaster, AL). Heptane, diethyl ether, and glacial acetic acid (60:40:2 by volume) were used for total phospholipid isolation. Bands were identified by 0.1% 8-anilino-1-naphthalene sulfonic acid spray under ultraviolet light. Total phospholipid fatty acids and internal standards (17:0 and 22:3n-3) were converted into fatty acid methyl esters with 14% boron trifluoride–methanol at 100°C for 1 hour, followed by quantification with gas chromatography–flame ionization detection. The concentration of each fatty acid was quantified by peak comparison to the internal standards and expressed as nmol/g brain or retina.

Statistical analysis

Data were analyzed using GraphPad Prism 6.01 (GraphPad Software, San Diego, CA). The values shown in the graphs are presented as means ± SD of at least three independent experiments. Statistical differences between groups were analyzed using a one-way analysis of variance (ANOVA) statistical test with Dunnett's multiple comparisons tests or two-tailed unpaired *t* tests; $P < 0.05$ was considered statistically significant.

SUPPLEMENTARY MATERIALS

Supplementary material for this article is available at http://advances.sciencemag.org/cgi/content/full/6/35/eaba7457/DC1

View/request a protocol for this paper from *Bio-protocol*.

REFERENCES AND NOTES

1. R. Daneman, A. Prat, The blood-brain barrier. *Cold Spring Harb. Perspect. Biol.* **7**, a020412 (2015).
2. G. Raviola, The structural basis of the blood-ocular barriers. *Exp. Eye Res.* **25**, 27–63 (1977).
3. T. S. Reese, M. J. Karnovsky, Fine structural localization of a blood-brain barrier to exogenous peroxidase. *J. Cell Biol.* **34**, 207–217 (1967).
4. S. Ayloo, C. Gu, Transcytosis at the blood-brain barrier. *Curr. Opin. Neurobiol.* **57**, 32–38 (2019).
5. J. Keaney, M. Campbell, The dynamic blood-brain barrier. *FEBS J.* **282**, 4067–4079 (2015).
6. C. Greene, M. Campbell, Tight junction modulation of the blood brain barrier: CNS delivery of small molecules. *Tissue Barriers* **4**, e1138017 (2016).
7. A. Ben-Zvi, B. Lacoste, E. Kur, B. J. Andreone, Y. Mayshar, H. Yan, C. Gu, Mfsd2a is critical for the formation and function of the blood-brain barrier. *Nature* **509**, 507–511 (2014).
8. D. Knowland, A. Arac, K. J. Sekiguchi, M. Hsu, S. E. Lutz, J. Perrino, G. K. Steinberg, B. A. Barres, A. Nimmerjahn, D. Agalliu, Stepwise recruitment of transcellular and paracellular pathways underlies blood-brain barrier breakdown in stroke. *Neuron* **82**, 603–617 (2014).
9. D. A. Antonetti, R. Klein, T. W. Gardner, Diabetic retinopathy. *N. Engl. J. Med.* **366**, 1227–1239 (2012).
10. I. Klaassen, C. J. F. Van Noorden, R. O. Schlingemann, Molecular basis of the inner blood-retinal barrier and its breakdown in diabetic macular edema and other pathological conditions. *Prog. Retin. Eye Res.* **34**, 19–48 (2013).
11. M. Kato, M. S. Patel, R. Levasseur, I. Lobov, B. H.-J. Chang, D. A. Glass II, C. Hartmann, L. Li, T.-H. Hwang, C. F. Brayton, R. A. Lang, G. Karsenty, L. Chan, *Cbfa1*-independent decrease in osteoblast proliferation, osteopenia, and persistent embryonic eye vascularization in mice deficient in Lrp5, a Wnt coreceptor. *J. Cell Biol.* **157**, 303–314 (2002).
12. Z. Wang, C.-H. Liu, S. Huang, J. Chen, Wnt signaling in vascular eye diseases. *Prog. Retin. Eye Res.* **70**, 110–133 (2019).
13. U. F. O. Luhmann, J. Lin, N. Acar, S. Lammel, S. Feil, C. Grimm, M. W. Seeliger, H.-P. Ham1mes, W. Berger, Role of the Norrie disease pseudoglioma gene in sprouting angiogenesis during development of the retinal vasculature. *Invest. Ophthalmol. Vis. Sci.* **46**, 3372–3382 (2005).
14. C. Toomes, L. Downey, Familial exudative vitreoretinopathy, autosomal dominant, in *GeneReviews*, R. A. Pagon, T. D. Bird, C. R. Dolan, K. Stephens, Eds. (University of Washington, 1993).
15. X. Ye, Y. Wang, J. Nathans, The Norrin/Frizzled4 signaling pathway in retinal vascular development and disease. *Trends Mol. Med.* **16**, 417–425 (2010).
16. J. Chen, A. Stahl, N. M. Krah, M. R. Seaward, J.-S. Joyal, A. M. Juan, C. J. Hatton, C. M. Aderman, R. J. Dennison, K. L. Willett, P. Sapieha, L. E. H. Smith, Retinal expression of Wnt-pathway mediated genes in low-density lipoprotein receptor-related protein 5 (Lrp5) knockout mice. *PLOS ONE* **7**, e30203 (2012).
17. Q. Xu, Y. Wang, A. Dabdoub, P. M. Smallwood, J. Williams, C. Woods, M. W. Kelley, L. Jiang, W. Tasman, K. Zhang, J. Nathans, Vascular development in the retina and inner ear: Control by Norrin and Frizzled-4, a high-affinity ligand-receptor pair. *Cell* **116**, 883–895 (2004).
18. H. L. Rehm, D.-S. Zhang, M. C. Brown, B. Burgess, C. Halpin, W. Berger, C. C. Morton, D. P. Corey, Z.-Y. Chen, Vascular defects and sensorineural deafness in a mouse model of Norrie disease. *J. Neurosci.* **22**, 4286–4292 (2002).
19. C. Y. Logan, R. Nusse, The Wnt signaling pathway in development and disease. *Annu. Rev. Cell Dev. Biol.* **20**, 781–810 (2004).
20. R. Nusse, H. Clevers, Wnt/β-catenin signaling, disease, and emerging therapeutic modalities. *Cell* **169**, 985–999 (2017).
21. R. T. Moon, A. D. Kohn, G. V. De Ferrari, A. Kaykas, WNT and β-catenin signalling: Diseases and therapies. *Nat. Rev. Genet.* **5**, 691–701 (2004).
22. M. Díaz-Coránguez, C. Ramos, D. A. Antonetti, The inner blood-retinal barrier: Cellular basis and development. *Vision Res.* **139**, 123–137 (2017).
23. S. Liebner, M. Corada, T. Bangsow, J. Babbage, A. Taddei, C. J. Czupalla, M. Reis, A. Felici, H. Wolburg, M. Fruttiger, M. M. Taketo, H. von Melchner, K. H. Plate, H. Gerhardt,

E. Dejana, Wnt/β-catenin signaling controls development of the blood-brain barrier. *J. Cell Biol.* **183**, 409–417 (2008).
24. J. M. Stenman, J. Rajagopal, T. J. Carroll, M. Ishibashi, J. M. Mahon, A. P. McMahon, Canonical Wnt signaling regulates organ-specific assembly and differentiation of CNS vasculature. *Science* **322**, 1247–1250 (2008).
25. R. Daneman, D. Agalliu, L. Zhou, F. Kuhnert, C. J. Kuo, B. A. Barres, Wnt/β-catenin signaling is required for CNS, but not non-CNS, angiogenesis. *Proc. Natl. Acad. Sci. U.S.A.* **106**, 641–646 (2009).
26. Y. Zhou, J. Nathans, Gpr124 controls CNS angiogenesis and blood-brain barrier integrity by promoting ligand-specific canonical wnt signaling. *Dev. Cell* **31**, 248–256 (2014).
27. C. Cho, P. M. Smallwood, J. Nathans, Reck and Gpr124 are essential receptor cofactors for Wnt7a/Wnt7b-specific signaling in mammalian CNS angiogenesis and blood-brain barrier regulation. *Neuron* **95**, 1056–1073.e5 (2017).
28. Y. Wang, A. Rattner, Y. Zhou, J. Williams, P. M. Smallwood, J. Nathans, Norrin/Frizzled4 signaling in retinal vascular development and blood brain barrier plasticity. *Cell* **151**, 1332–1344 (2012).
29. W. Huang, Q. Li, M. Amiry-Moghaddam, M. Hokama, S. H. Sardi, M. Nagao, M. L. Warman, B. R. Olsen, Critical endothelial regulation by LRP5 during retinal vascular development. *PLOS ONE* **11**, e0152833 (2016).
30. J. Chen, A. Stahl, N. M. Krah, M. R. Seaward, R. J. Dennison, P. Sapieha, J. Hua, C. J. Hatton, A. M. Juan, C. M. Aderman, K. L. Willett, K. I. Guerin, A. Mammoto, M. Campbell, L. E. H. Smith, Wnt signaling mediates pathological vascular growth in proliferative retinopathy. *Circulation* **124**, 1871–1881 (2011).
31. F. Benz, V. Wichitnaowarat, M. Lehmann, R. F. Germano, D. Mihova, J. Macas, R. H. Adams, M. M. Taketo, K.-H. Plate, S. Guérit, B. Vanhollebeke, S. Liebner, Low wnt/β-catenin signaling determines leaky vessels in the subfornical organ and affects water homeostasis in mice. *eLife* **8**, e43818 (2019).
32. Y. Wang, C. Cho, J. Williams, P. M. Smallwood, C. Zhang, H. J. Junge, J. Nathans, Interplay of the Norrin and Wnt7a/Wnt7b signaling systems in blood-brain barrier and blood-retina barrier development and maintenance. *Proc. Natl. Acad. Sci. U.S.A.* **115**, E11827–E11836 (2018).
33. L. N. Nguyen, D. Ma, G. Shui, P. Wong, A. Cazenave-Gassiot, X. Zhang, M. R. Wenk, E. L. K. Goh, D. L. Silver, Mfsd2a is a transporter for the essential omega-3 fatty acid docosahexaenoic acid. *Nature* **509**, 503–506 (2014).
34. N. M. O'Brown, S. G. Megason, C. Gu, Suppression of transcytosis regulates zebrafish blood-brain barrier function. *eLife* **8**, (2019).
35. B. J. Andreone, B. W. Chow, A. Tata, B. Lacoste, A. Ben-Zvi, K. Bullock, A. A. Deik, D. D. Ginty, C. B. Clish, C. Gu, Blood-brain barrier permeability is regulated by lipid transport-dependent suppression of caveolae-mediated transcytosis. *Neuron* **94**, 581–594.e585 (2017).
36. J.-Z. Wang, N. Xiao, Y.-Z. Zhang, C.-X. Zhao, X.-H. Guo, L.-M. Lu, Mfsd2a-based pharmacological strategies for drug delivery across the blood-brain barrier. *Pharmacol. Res.* **104**, 124–131 (2016).
37. N. F. Schäfer, U. F. O. Luhmann, S. Feil, W. Berger, Differential gene expression in *Ndph*-knockout mice in retinal development. *Invest. Ophthalmol. Vis. Sci.* **50**, 906–916 (2009).
38. M. M. Afifi, L. A. Austin, M. A. Mackey, M. A. El-Sayed, XAV939: From a small inhibitor to a potent drug bioconjugate when delivered by gold nanoparticles. *Bioconjug. Chem.* **25**, 207–215 (2014).
39. M. A. Oosterwegel, M. L. van de Wetering, F. C. Holstege, H. M. Prosser, M. J. Owen, H. C. Clevers, TCF-1, a T cell-specific transcription factor of the HMG box family, interacts with sequence motifs in the TCRβ and TCRδ enhancers. *Int. Immunol.* **3**, 1189–1192 (1991).
40. B. W. Chow, C. Gu, Gradual suppression of transcytosis governs functional blood-retinal barrier formation. *Neuron* **93**, 1325–1333.e3 (2017).
41. M. Bastiani, R. G. Parton, Caveolae at a glance. *J. Cell Sci.* **123**, 3831–3836 (2010).
42. T. M. Williams, M. P. Lisanti, The caveolin proteins. *Genome Biol.* **5**, 214 (2004).
43. A. Guemez-Gamboa, L. N. Nguyen, H. Yang, M. S. Zaki, M. Kara, T. Ben-Omran, N. Akizu, R. O. Rosti, B. Rosti, E. Scott, J. Schroth, B. Copeland, K. K. Vaux, A. Cazenave-Gassiot, D. Q. Y. Quek, B. H. Wong, B. C. Tan, M. R. Wenk, M. Gunel, S. Gabriel, N. C. Chi, D. L. Silver, J. G. Gleeson, Inactivating mutations in MFSD2A, required for omega-3 fatty acid transport in brain, cause a lethal microcephaly syndrome. *Nat. Genet.* **47**, 809–813 (2015).
44. Z. Zhao, A. R. Nelson, C. Betsholtz, B. V. Zlokovic, Establishment and dysfunction of the blood-brain barrier. *Cell* **163**, 1064–1078 (2015).
45. J. Mazzoni, J. R. Smith, S. Shahriar, T. Cutforth, B. Ceja, D. Agalliu, The Wnt inhibitor Apcdd1 coordinates vascular remodeling and barrier maturation of retinal blood vessels. *Neuron* **96**, 1055–1069.e6 (2017).
46. B. Engelhardt, S. Liebner, Novel insights into the development and maintenance of the blood-brain barrier. *Cell Tissue Res.* **355**, 687–699 (2014).
47. B. H. Wong, J. P. Chan, A. Cazenave-Gassiot, R. W. Poh, J. C. Foo, D. L. A. Galam, S. Ghosh, L. N. Nguyen, V. A. Barathi, S. W. Yeo, C. D. Luu, M. R. Wenk, D. L. Silver, Mfsd2a is a transporter for the essential ω-3 fatty acid docosahexaenoic acid (DHA) in eye and is important for photoreceptor cell development. *J. Biol. Chem.* **291**, 10501–10514 (2016).
48. E. S. Lobanova, K. Schuhmann, S. Finkelstein, T. R. Lewis, M. A. Cady, Y. Hao, C. Keuthan, J. D. Ash, M. E. Burns, A. Shevchenko, V. Y. Arshavsky, Disrupted blood-retina lysophosphatidylcholine transport impairs photoreceptor health but not visual signal transduction. *J. Neurosci.* **39**, 9689–9701 (2019).
49. Y. Wang, M. F. Sabbagh, X. Gu, A. Rattner, J. Williams, J. Nathans, Beta-catenin signaling regulates barrier-specific gene expression in circumventricular organ and ocular vasculatures. *eLife* **8**, e43257 (2019).
50. A. Rattner, Y. Wang, Y. Zhou, J. Williams, J. Nathans, The role of the hypoxia response in shaping retinal vascular development in the absence of Norrin/Frizzled4 signaling. *Invest. Ophthalmol. Vis. Sci.* **55**, 8614–8625 (2014).
51. Z. Wang, C.-H. Liu, Y. Sun, Y. Gong, T. L. Favazza, P. C. Morss, N. J. Saba, T. W. Fredrick, X. He, J. D. Akula, J. Chen, Pharmacologic activation of wnt signaling by lithium normalizes retinal vasculature in a murine model of familial exudative vitreoretinopathy. *Am. J. Pathol.* **186**, 2588–2600 (2016).
52. J. E. Preston, N. Joan Abbott, D. J. Begley, Transcytosis of macromolecules at the blood-brain barrier. *Adv. Pharmacol.* **71**, 147–163 (2014).
53. N. Bien-Ly, Y. J. Yu, D. Bumbaca, J. Elstrott, C. A. Boswell, Y. Zhang, W. Luk, Y. Lu, M. S. Dennis, R. M. Weimer, I. Chung, R. J. Watts, Transferrin receptor (TfR) trafficking determines brain uptake of TfR antibody affinity variants. *J. Exp. Med.* **211**, 233–244 (2014).
54. P. Oh, P. Borgström, H. Witkiewicz, Y. Li, B. J. Borgström, A. Chrastina, K. Iwata, K. R. Zinn, R. Baldwin, J. E. Testa, J. E. Schnitzer, Live dynamic imaging of caveolae pumping targeted antibody rapidly and specifically across endothelium in the lung. *Nat. Biotechnol.* **25**, 327–337 (2007).
55. W. Schubert, P. G. Frank, B. Razani, D. S. Park, C. W. Chow, M. P. Lisanti, Caveolae-deficient endothelial cells show defects in the uptake and transport of albumin *in vivo*. *J. Biol. Chem.* **276**, 48619–48622 (2001).
56. C. T. Chen, A. P. Kitson, K. E. Hopperton, A. F. Domenichiello, M.-O. Trépanier, L. E. Lin, L. Ermini, M. Post, F. Thies, R. P. Bazinet, Plasma non-esterified docosahexaenoic acid is the major pool supplying the brain. *Sci. Rep.* **5**, 15791 (2015).
57. J. Zhou, X. Chi, M. Cheng, X. Huang, X. Liu, J. Fan, H. Xu, T. Lin, L. Shi, C. Qin, W. Yang, Zika virus degrades the ω-3 fatty acid transporter Mfsd2a in brain microvascular endothelial cells and impairs lipid homeostasis. *Sci. Adv.* **5**, eaax7142 (2019).
58. C. Betsholtz, Physiology: Double function at the blood-brain barrier. *Nature* **509**, 432–433 (2014).
59. I. Mäger, A. H. Meyer, J. Li, M. Lenter, T. Hildebrandt, G. Leparc, M. J. A. Wood, Targeting blood-brain-barrier transcytosis—Perspectives for drug delivery. *Neuropharmacology* **120**, 4–7 (2017).
60. Y. Tomita, Z. Fu, Z. Wang, B. Cakir, S. S. Cho, W. Britton, Y. Sun, A. Hellström, S. Talukdar, L. E. H. Smith, Long-acting FGF21 inhibits retinal vascular leakage in in vivo and in vitro models. *Int. J. Mol. Sci.* **21**, 1188 (2020).

Acknowledgments: We thank L. E. H. Smith for very helpful discussion and critical reading of the manuscript, as well as R. Duran, P. Morss, S. Meng, S. Burnim, and A. Poblete for excellent technical assistance. We also thank C. Gu, B. Andreone, B. W. Chow for their assistance with EM protocols; M. Ericsson and L. M Trakimas at Harvard Medical School Electron Microscopy Core Facility for their assistance with EM sample processing and imaging; E. Engelbrecht and T. Hla for their technical help; and D. L. Silver for providing MFSD2A antibodies. **Funding:** This work was supported by NIH grants (R01 EY028100 and EY024963), BrightFocus Foundation, Boston Children's Hospital Ophthalmology Foundation, Massachusetts Lions Eye Research Fund Inc., and Alcon Research Institute (to J.C.). Z.W. and C.-H.L. were supported by Knights Templar Eye Foundation Career Starter Grants. Y.S. was supported by NIH (R01 EY030140, R01 EY029238), BrightFocus Foundation, and Boston Children's Hospital Ophthalmology Foundation. Y.T. was supported by Manpei Diabetic Foundation. X.H. acknowledges support by NIH (1R35GM134953) and by Boston Children's Hospital Intellectual and Developmental Disabilities Research Center (P30 HD-18655). X.H. is an American Cancer Society Research Professor. **Author contributions:** Z.W. and J.C. conceived and designed the study and wrote the manuscript. Z.W., C.-H.L., S.H., W.R.B., S.S.C., and C.T.C. performed experiments and collected and analyzed the data; Z.F., Y.T., C.T.C., Y.S., J.-x.M., and X.H. shared reagents and resources and provided expert advice; all authors edited and approved the manuscript. **Competing interests:** The authors declare that they have no competing interests. **Data and materials availability:** All data needed to evaluate the conclusions in the paper are present in the paper and/or the Supplementary Materials. Additional data related to this paper may be requested from the authors.

Submitted 31 December 2019
Accepted 15 July 2020
Published 28 August 2020
10.1126/sciadv.aba7457

Citation: Z. Wang, C.-H. Liu, S. Huang, Z. Fu, Y. Tomita, W. R. Britton, S. S. Cho, C. T. Chen, Y. Sun, J.-x. Ma, X. He, J. Chen, Wnt signaling activates MFSD2A to suppress vascular endothelial transcytosis and maintain blood-retinal barrier. *Sci. Adv.* **6**, eaba7457 (2020).